Experimental Results Using Satellite Illuminator for Passive Bistatic Radar

Jeffrey D. Ouellette, David J. Dowgiallo, and Joseph F. Helmboldt
U.S. Naval Research Laboratory
4555 Overlook Ave. SW, Washington, DC
USA

jeffrey.ouellette@nrl.navy.mil

ABSTRACT

Passive, bistatic radar offers an attractive method for remotely detecting and imaging targets without the requirement of a dedicated transmitter. Passive radar systems are usually cheaper than their active counterparts, which easily allows for multi-sensor networks. Furthermore, passive radar systems are difficult to detect and jam. With these advantages come several challenges, however. Bistatic ranging is often a more difficult problem than monostatic ranging since the bistatic range depends on the position of the target relative to the transmitter and the receiver(s). Also, passive radars have no control over the transmitted waveform and are forced to utilize signals of opportunity. These non-cooperative signals of opportunity are typically communications signals which do not usually offer the high transmit power or wide bandwidth of a conventional monostatic radar. This study describes a new passive radar system utilizing a non-cooperative, satellite-based illuminator. Capabilities of this new system are initially demonstrated with Doppler imaging results from land-, sea-, and air-based targets.

1.0 INTRODUCTION

Passive radar using terrestrial transmitters has been studied for the past several decades. Given their significantly lower cost, passive radar technology has been proposed for a wide variety of applications, including airport security and harbor surveillance [1,2]. When compared to the number of studies involving the use of terrestrial emitters, relatively few studies have explored the use of satellite-based illuminators for passive radar [3,4]. Furthermore, existing studies of reflections from satellite-based transmitters typically focus either on specular scattering or scattering within the plane of incidence. Recent literature suggests that moving to out-of-plane geometries offers better flexibility and fosters the development of multi-static and bistatic multiple-input/multiple-output (MIMO) networks [3].

The system described herein utilizes signals transmitted by the XM/Sirius satellite radio constellation as a network of illuminators-of-opportunity. Reflections of XM/Sirius signals from various targets are processed into range-Doppler maps for several different targets, ranges, and bistatic geomeries.

2.0 OVERVIEW OF BISTATIC RADAR

Bistatic radar presents the opportunity to view targets at unique angles which are not achievable with monostatic systems. This section seeks to clarify the viewing geometries available to a bistatic radar system, as well as the benefits and drawbacks of various bistatic configurations.

Figure 2-1 shows a basic illustration of the bistatic radar geometry, including one reference and one surveillance channel. A reduction in the bistatic angle β between the transmitter and receiver in the illustration demonstrates a geometry towards an "over-the-shoulder" configuration, which mimics the behavior of a continuous-wave monostatic radar. Such a configuration is often ideal in that self-interference from the direct signal is limited and the bistatic Doppler can be maximized. Figure 2-1 illustrates the relationship between the bistatic geometry and the Doppler shift of the reflection from the target. Note that this Doppler shift can change significantly if the

target accelerates, decelerates, or performs a maneuver which changes its aspect angle from the radar's perspective.

In regards to bistatic radar cross section (RCS), the three broadly-defined angular regions considered in literature are the pseudo-monostatic, the bistatic, and the forward scatter mode, each of which is defined by a range of the bistatic angle β. The pseudo-monostatic is the case where the bistatic angle is small, whereas the forward scatter mode is the case where $\beta > 90°$. The Crispin and Siegel monostatic-bistatic equivalence theorem can be applied to the pseudo-monostatic region, with a variation developed by Kell being applied to more complex targets [5]. The targets of interest for this paper were viewed in pseudo-monostatic and bistatic modes, where $\beta < 90°$.

3.0 SIGNAL PROCESSING OVERVIEW

The ability for a radar system to separate targets is characterized by the system's range and Doppler resolution. Range resolution determines the ability to separate closely spaced targets, while Doppler resolution provides separation of velocity for multiple targets. The ambiguity function provides a matched filter response of a reference signal and a surveillance channel from a common transmitter, and from this range and Doppler resolution can be determined [6]. The ambiguity function (AF) computed over a certain Coherent Processing Interval (CPI) of T_{CPI} for a reference channel $u_{reference}(t)$ and a surveillance channel $u_{surveillance}(t)$ is defined as

$$|\chi(\tau, f_d)| = \left| \int_0^{T_{CPI}} u_{reference}(t) u^*_{surveillance}(t+\tau) e^{j2\pi f_d t}\, dt \right|.$$

The ambiguity function provides performance information on a signal of interest in terms of frequency and temporal resolution. The self-ambiguity function (SAF) describes the correlation of a signal in time (t) and frequency (f_d) with a copy of itself; the self-ambiguity function is simply the case where $u_{surveillance} = u_{reference}$. The SAF of an XM3-B transmission, centered at 2344.05 GHz, is shown in Figure 3-1. A pseudo-random, high-bandwidth, coherent signal achieves an ideal, "thumbtack"-like SAF, where few range/Doppler ambiguities exist. Of note is that for this study, the content of the signal is not decoded, but rather processed as a continuous data stream, much like conventional continuous-wave radar.

3.1 The XM Radio Signal

The XM/Sirius radio constellation currently consists of multiple satellites positioned in both geosynchronous geostationary orbits. The measurements described herein focus solely on the XM3 satellite, located at 85°W, due to its stability in geostationary orbit (the satellite does not need to be tracked) and its relative proximity to the study areas on the East coast of the United States. XM3 transmits data in two discrete frequency bands: XM3A, centered at 2333.47 GHz, and XM3B, centered at 2344.05 GHz. XM3A and XM3B are both quadrature phase-shift key (QPSK) modulated, symbol rate of 1.64 MHz, with each band having a half-power bandwidth of 1.84 MHz. The XM satellite and terrestrial frequency spectrum is shown in Figure 3-1. The satellite's effective isotropic radiative power is 68.5 dBW. Note the terrestrial repeater bandwidth allocation that is located in the middle of the band, and which can contain significant signal power in city areas. XM terrestrial repeaters are tower-based transponders designed to boost the XM signal in urban areas in order to combat the effects of multipath, which can degrade the signal received by XM Radio customers. These repeaters manifest themselves as radio frequency interference (RFI) to a passive radar using the satellite as an illuminator, however the repeaters themselves could potentially be used as an independent terrestrial emitter for passive radar applications.

3.2 Doppler Processing in Passive Bistatic Radar

As stated in Section 3.0, the CPI is defined as the time over which the cross-correlation between the reference and surveillance channels for each point in the bistatic range-Doppler map. It is desirable to coherently integrate

for as long as possible to maximize integration processing gain, however a target whose Doppler shift changes rapidly with time cannot be detected using a long CPI. The maximum allowable CPI will be ultimately determined by how quickly the target is expected to migrate in bistatic range-Doppler space.

Incoherent integration was employed in this study by simply summing a number of instantaneous range-Doppler maps generated by coherent processing. Incoherent averaging results in an increased signal-to-noise ratio (SNR) at the cost of potentially "smearing" the target in Doppler space due to temporal Doppler scintillations. This smearing effect is more pronounced for faster-moving targets and longer incoherent integration intervals.

4.0 THE B.I.S.C.U.I.T. RECEIVER, AND DATA ACQUISITION SYSTEMS

The Bistatic, Coherent, Unobtrusive Imager and Tracker (BISCUIT) receiver was designed to receive XM satellite radio signals and their reflections from manmade targets. The system was built with the intention of using baseline interferometry techniques, thus each receiving channel was phase matched to within 3 degrees. First-stage low-noise amplifiers (LNAs) were kept external to the BISCUIT itself so that the LNAs could be connected directly to the receiving antennas. In additional two commercially-available data acquisition systems were separately used with the BISCUIT in order to record, digitize, and store received data.

4.1 Receiver Design Phases

Two design iterations of the BISCUIT have been used to generate the results in the next section. Both design iterations were constructed entirely from commercial, off-the-shelf (COTS) components. Designing the system in this manner maintains a low cost for each receiver channel and allows for extensibility to multiple receiver channels. Each iteration of the BISCUIT was used in conjunction with external low-noise amplifiers (LNAs) which were connected directly to the receiving antennas. Signals received by the BISCUIT were amplified, filtered, and mixed to an intermediate frequency (IF). IF data were then passed to the data acquisition system for digitization and storage. The stored digital data were then processed offline for target detection, tracking, and/or imaging. A generalized block diagram of the experimental setup including the BISCUIT and data acquisition system is shown in Figure 4-1.

4.1.1 BISCUIT 1.0 and the Signatec System

BISCUIT 1.0 was the first (legacy) design iteration of BISCUIT, offering up to three receiving channels (one reference channel and up to two surveillance channels). Received radio frequency (RF) signals were passed through several filtering and amplification stages and were mixed down to an intermediate frequency (IF). The BISCUIT 1.0 receiver, including the front-end LNAs, had a bandwidth of 2 MHz, an end-to-end system gain of 76 dB and a noise figure of 1.5 dB.

The Signatec data acquisition system was used exclusively in conjunction with the first (legacy) design iteration of the BISCUIT receiver. Output files from the digitizer are in the form of 8-bit unsigned integers. The digitizer could use 8 effective bits, but in order to avoid saturation/clipping, the full range of the digitizer was seldom used experimentally. The system was capable of operating at several different sampling rates. For these experiments, a sampling rate of 62.50 Ms/s was used with the Signatec system.

4.1.2 BISCUIT 2.0 and the Picoscope System

BISCUIT 2.0 was the second (new) design iteration of BISCUIT, offering up to seven receiving channels (one reference channel and up to six surveillance channels). Received RF signals were passed through several filtering and amplification stages and were mixed down to an IF. The BISCUIT 2.0 receiver, including the front-end LNAs, had a bandwidth of 2 MHz, an end-to-end system gain of 96 dB and a noise figure of 1.5 dB.

The Picoscope data acquisition system was used exclusively in conjunction with the second (current) design iteration of the BISCUIT receiver. Output files from the digitizer are in the form of 16-bit signed integers. It was

found through lab testing that the Picoscope digitizer could realistically achieve roughly 10.5 effective bits. The system was capable of operating at several different sampling rates. For these experiments, a sampling rate of 26.67 Ms/s was used with the Picoscope system.

5.0 DOPPLER IMAGERY OF MOVING TARGETS

The results in this section include imagery of manmade targets, and were produced by offline data processing. These data include reflections from three polarizations: horizontal (H) polarization, Left-Hand Circular Polarization (LHCP) and Right-Hand Circular Polarization (RHCP). The CPI and Incoherent Processing Interval (IPI) were selected based on the target being observed, the target velocity, the bistatic geometry, and the approximate dwell time on the target.

5.1 Ground Vehicles

Data for land-based targets were collected locally at NRL-DC (Naval Research Laboratory - District of Columbia) using BISCUIT 1.0. H-polarized and RHCP reflector antennas were used for the surveillance channels, while the reference channel antenna was an H-polarized grid reflector. Signals measured using BISCUIT 1.0 were recorded, digitized and stored using the Signatec data acquisition system. Figure 5-1 shows a top-down illustration of the experimental setup and an image of a vehicle whose Doppler response was measured using BISCUIT 1.0.

Figure 5-2 shows a sample time-Doppler image of a golf cart. The vehicle is moving at a constant velocity of about 15 MPH through the surveillance antenna beams at close range. During data collection, the vehicle is less than 30 meters from the receiving antennas at all times. As such, the resulting Doppler image is processed for one fixed range; the y-axis corresponds to time evolution in seconds. It is easily seen from Figure 5-2 that the signal strength and Doppler shift of bistatic reflections from the golf cart change rapidly over time. This is due to the relationship between the position and velocity of the target and the positions of the transmitter and receiver, which is highlighted in Section 2.0.

Given the relatively constant velocity of the golf cart, a comparison could be made of the H-polarized and LHCP returns for a one-dimensional inverse synthetic aperture radar (ISAR) image of the golf cart. Figure 5-3 displays such a comparison in the form of the ISAR cross-range profiles for both polarizations versus time. The ISAR profile is produced using the motion of the target relative to the surveillance antenna and shows the locations of strong scatterers on the target by plotting the scattered power as a function of cross-range. In this analysis, it is assumed that the target exhibits a linear time-Doppler relationship. Note the lobe in the left side of the LHCP profile may be due to the non-linear motion of the golf cart as it moves away from the surveillance antenna boresight.

5.2 Aircraft

In a continuation of the local field campaign at NRL-DC, BISCUIT 1.0 was used in an attempt to detect and track aircraft of their landing approach to Ronald Reagan National airport. LHCP and RHCP dish antennas were used for the surveillance channels, while the reference channel antenna was a horizontally-polarized grid reflector. Signals measured using BISCUIT 1.0 were recorded, digitized and stored using the Signatec data acquisition system. Figure 5-4 shows a top-down illustration of the experimental setup.

Figure 5-5 shows a sample range-Doppler image for one of the commercial aircraft detected by BISCUIT 1.0 at the NRL-DC campaign. Though no “truth” data was recorded for this aircraft, several other planes were also detected on approximately the same landing trajectory. Each plane shows up at roughly the same bistatic range-Doppler position, and is detected by both the RHCP and LHCP surveillance channels. Given the high velocity of the aircraft being imaged (on the order of 80 m/s) and the close range at which they were detected (less than 1 km), the aircraft migrate rapidly through bistatic range-Doppler space. Because of this rapid migration, the CPI

was limited to 67 milliseconds in order to prevent Doppler smearing (and therefore a missed detection or dropped track).

LHCP and RHCP reflections provide information on the structure of the target being observed. Because a circularly-polarized wave switches its handedness each time it bounces off of a reflective surface, the LHCP XM Radio signal becomes RHCP when it experiences a single-bounce reflected and remains LHCP when it experiences a double-bounce reflection. It was found that single-bounce (RHCP) reflections could be orders of magnitude weaker than double-bounce (LHCP) reflections from the aircraft observed in our configuration. For the RHCP reflection, the aircraft's SNR is 14.9 dB while for the LHCP reflection, the aircraft's SNR is 16.2 dB. In other images, SNR differences between LHCP and RHCP reflections could be greater by orders of magnitude. This is likely due to the strong double-bounce reflections produced by interactions between the tail section, wings, engines, and fuselage of the aircraft. By comparison, single-bounce reflections from the aircraft are expected to be relatively weak, especially considering the oblique angle of illuminator incidence. It was furthermore noticed that as the track of the aircraft was dropped in one polarization (due to insufficient SNR), it was usually picked up by the opposite polarization. This promotes the use of multiple polarization configurations for the detection and tracking of targets.

5.3 Watercraft

BISCUIT 2.0 was implemented in another experimental field campaign at NRL-CBD (Naval Research Laboratory - Chesapeake Bay Detachment). The goal of this experiment was to detect and track ship traffic in the Chesapeake Bay in order to test the new receiver hardware and software. H-polarized waveguide horn antennas were used for the surveillance channels, while the reference channel antenna was an H-polarized grid reflector. Signals measured using BISCUIT 2.0 were recorded, digitized and stored using the Picoscope data acquisition system. The digitally-recorded data was processed offline into range-Doppler images. Figure 5-6 shows a top-down illustration of the experimental setup.

Figure 5-7 displays a range-Doppler map showing simultaneous detections for three ships traveling through the Chesapeake Bay. According to concurrent Automated Information System (AIS) data, the nearest target was a tugboat pushing a barge, which was 6.7 km away from the experimental setup, moving at a speed of 4.9 m/s. The second-nearest target was a large cargo ship 9.4 km away, moving at a speed of 9.2 m/s. The furthest target was a tugboat pushing a barge 10.4 km away, moving at a speed of 1.0 m/s. Note that due to the long incoherent integration time, the fast-moving cargo ship is slightly blurred in Doppler space. The signal-to-noise ratios of the near, medium, and far targets are 18.3 dB, 13.2 dB, and 21.2 dB respectively.

6.0 CONCLUSIONS

Passive, bistatic radar offers a low-cost approach for remotely sensing targets without the requirement for a dedicated transmitter. Satellite-based transmitters are particularly attractive for this purpose given the wide area of coverage and oblique incidence angles which they provide. This study presented target detection results for a passive, bistatic radar systems using a satellite-based illuminator. The system has been demonstrated to be capable of detecting ground-, air-, and sea-based targets for a variety of ranges and bistatic geometries. During these experiments, the system has shown its capacity to form ISAR images of moving vehicles, detect fast-moving targets, and simultaneously image multiple targets at ranges on the order of several kilometers. Results presented herein show that passive, bistatic radar using satellite-based transmitters offers a flexible, viable method for detecting, tracking, and imaging manmade targets in many environments and geometries.

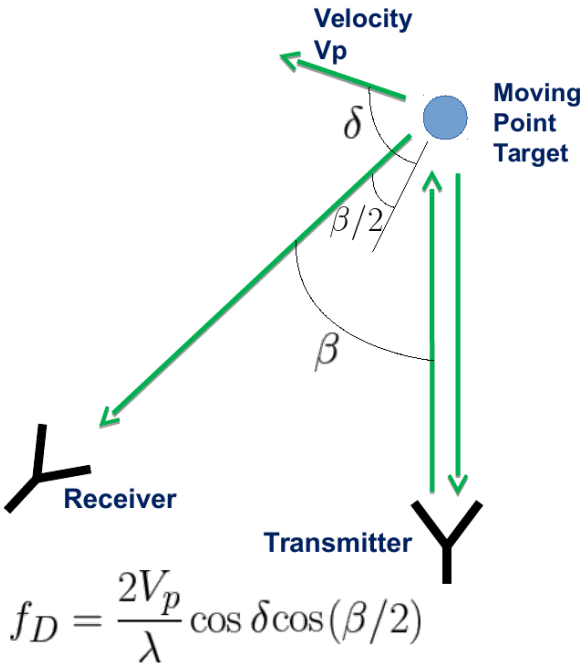

Figure 2-1: Bistatic geometry, target velocity, and Doppler relationship.

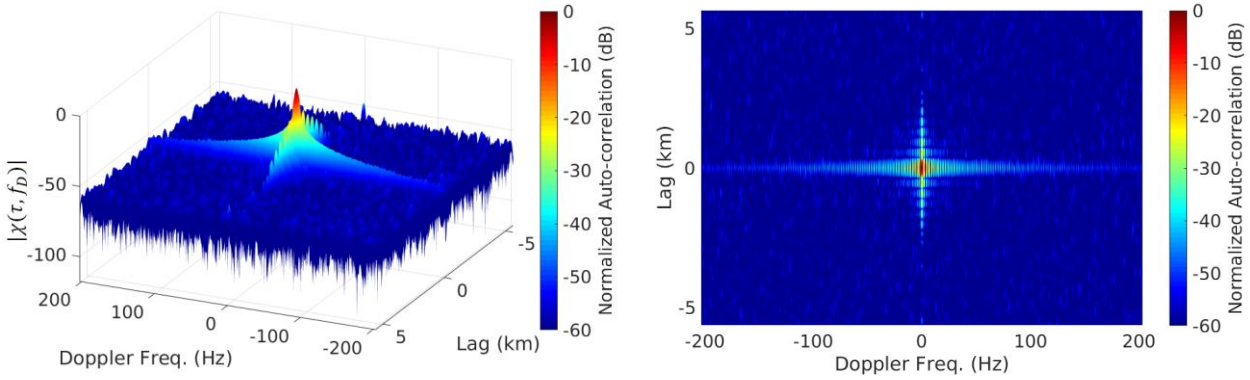

Figure 3-1: Self ambiguity plot of XM3-B satellite data as recorded in field experiment by the reference channel. This plot was created using a CPI of 629 milliseconds, resulting in a Doppler resolution of 1.59 Hz. The range resolution is driven by the signal bandwidth and bistatic geometry. In this configuration, the range resolution is about 382 meters. Note that the range resolution will improve in the case of an over-the-shoulder bistatic geometry.

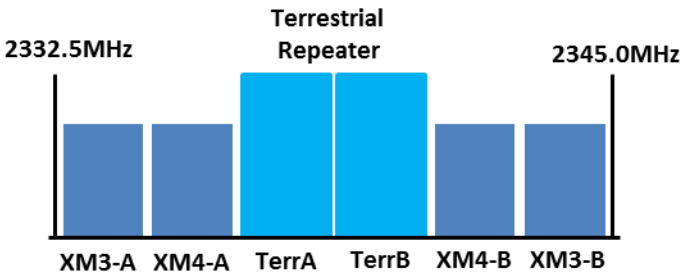

Figure 3-2: Diagram of XM satellite and terrestrial frequency bands.

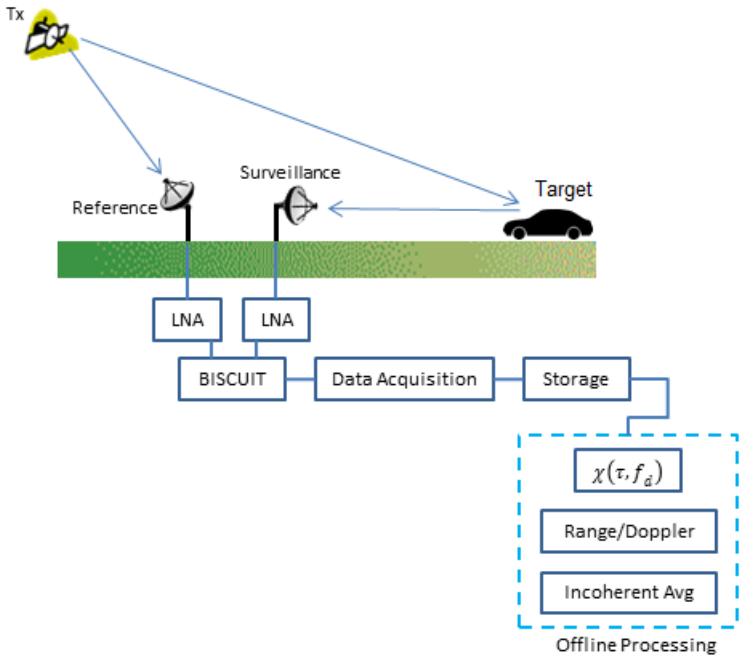

Figure 4-1: Bistatic geometry and data processing using XM Radio signals.

Figure 5-1: (Left) A top-down illustration of the measurement geometry for passive radar detection of ground vehicles at NRL-DC. (Right) A picture of the golf cart whose bistatic Doppler response is shown in Figure 5-2.

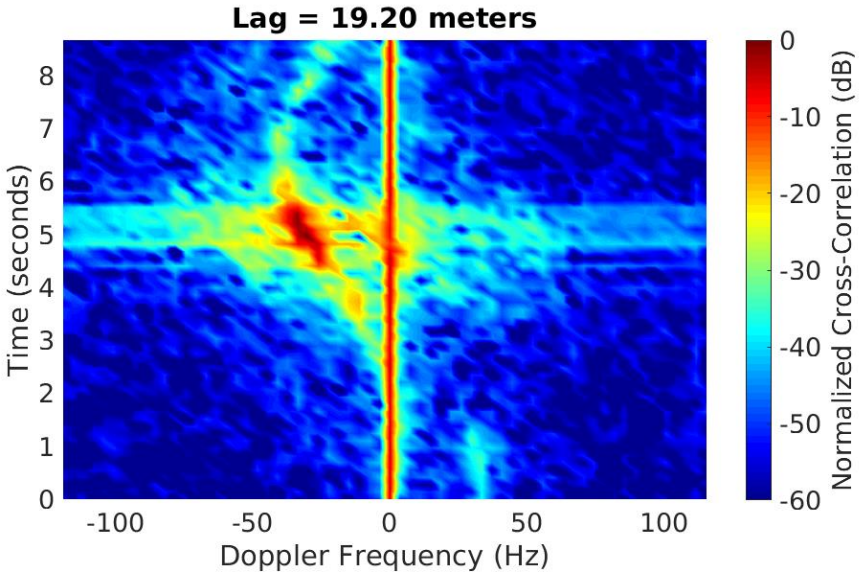

Figure 5-2: A bistatic time-Doppler image of a moving golf cart. The image corresponds to a fixed bistatic delay of 19.2 meters – this is the delay length between the surveillance and reference channels. This image was generated using a CPI of 268 milliseconds.

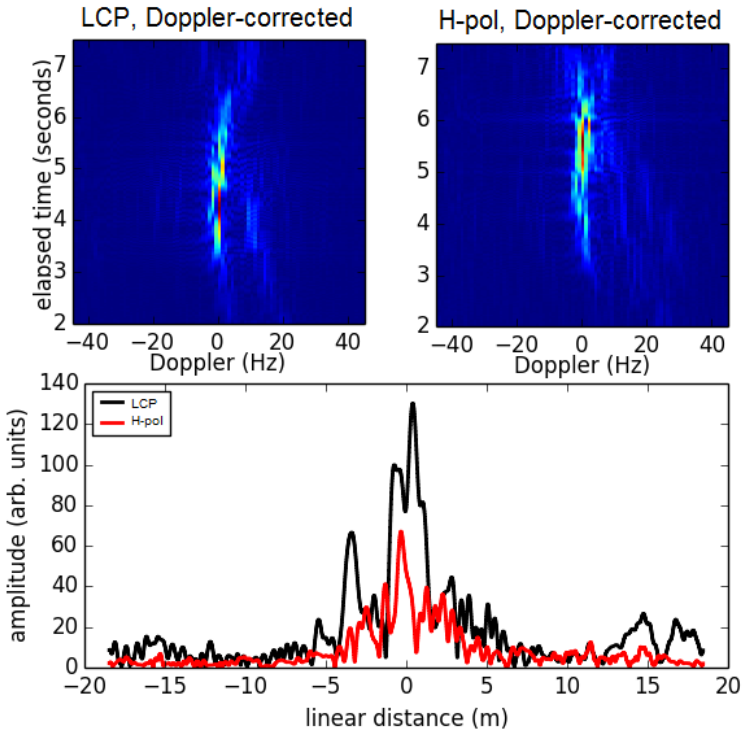

Figure 5-3: Top of figure: Doppler-correct images of golf cart image for horizontally-polarized (H-pol) and LCP reflections. Bottom of figure: a cross-range profile of the golf cart for both polarizations, derived from the Doppler-corrected images.

Figure 5-4: A top-down illustration of the measurement geometry for passive radar detection of aerial vehicles at the NRL-DC LASR facility.

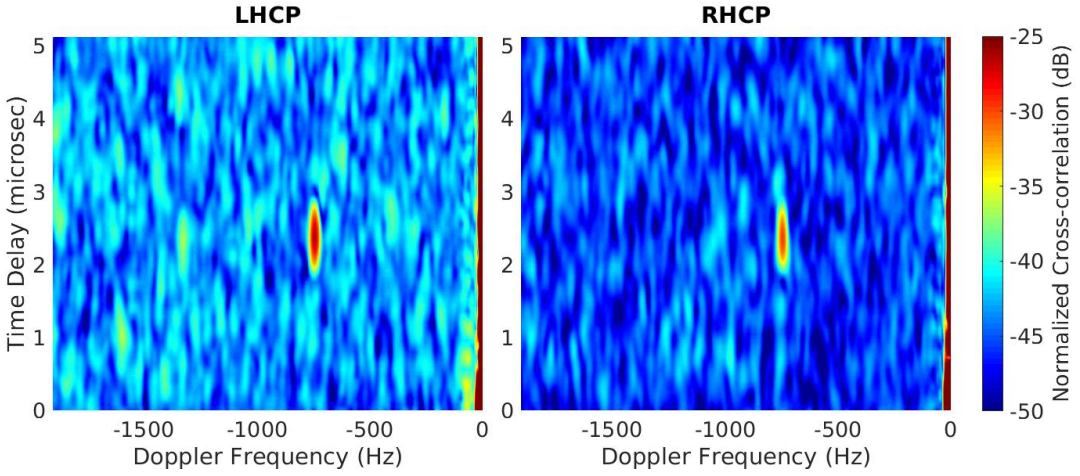

Figure 5-5: A normalized, integrated range-Doppler map of a commercial aircraft detected using reflections from the XM satellite radio signal. This image was produced using a CPI of 67 milliseconds and an IPI of 1 second. In this snapshot, the aircraft is located less than 1 km from the surveillance antenna.

Figure 5-6: Top-down view of the bistatic geometry employed to image ship traffic at NRL-CBD using the BISCUIT 2.0 system. The yellow dot represents the physical location of the receiver and the reference / surveillance antennas. The green arrow shows the azimuth pointing direction of the reference antenna, while the yellow arrows shows the azimuth pointing direction of the surveillance antenna.

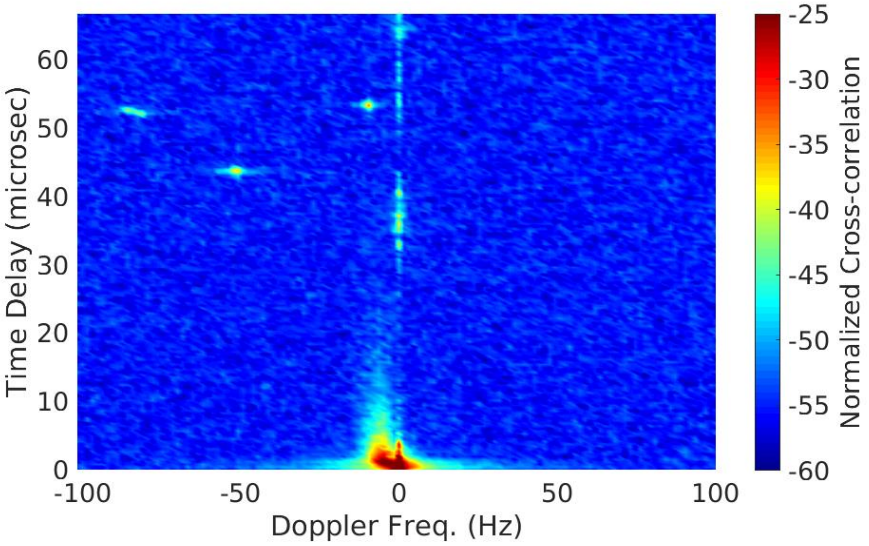

Figure 5-7: A normalized, integrated range-Doppler map of three ships traveling through the Chesapeake Bay, imaged from NRL-CBD. The three ships include one large cargo vessel and two tugboats, both of which were pushing barges. This image was produced using a CPI of 629 milliseconds and an IPI of 4.404 seconds. Note the fast-moving cargo ship has a lower SNR than the slower-moving tugboats due to Doppler smearing.

[1] Falcone, P., *et al.*: "Active and passive radar sensors for airport security" (*Tyrrhenian Advances in Radar and Remote Sensing*, Naples, Italy, 2012).

[2] O'Hagan, D. W., *et al.*: "Passive Bistatic Radar (PBR) for harbour protection applications" (*IEEE Radar Conference*, Atlanta, Georgia, USA, 2012).

[3] Barott, W. C. and Butka, B.: "SABER-TDA: passive coherent location of aircraft using XM-Radio and a small ground station" (*IEEE Radar Conference*, Atlanta, Georgia, USA, 2012).

[4] Glennon, E. P., Dempster, A. G., and Rizos, C.: "Feasibility of air target detection using GPS as a bistatic radar" (*Journal of Global Positioning Systems*, 2006).

[5] Willis, N.J.: "Bistatic Radar" (SciTech Publishing, Raleigh, NC, 2005).

[6] Peebles P.Z. Jr: "Radar Principles" (Wiley-Interscience, NY, 1998).